Engineering xxx (xxxx) xxx

Contents lists available at ScienceDirect

Engineering

journal homepage: www.elsevier.com/locate/eng

Research
Civil Engineering—Article

Dynamic Response of Full-Section Asphalt Concrete Waterproof Layer on Ballastless Tracks Employing Fractional-Order Modeling

Gang Xu [a,b], You Wu [c], Wei Huang [a,*], Yuefeng Shi [d], Tianling Wang [e], Degou Cai [d], Jinghong Tan [a], Xianhua Chen [a,*]

[a] School of Transportation, Southeast University, Nanjing 211189, China
[b] Key Laboratory of Transport Industry of Comprehensive Transportation Theory (Nanjing Modern Multimodal Transportation Laboratory), Nanjing 211135, China
[c] Section of Railway Engineering, Delft University of Technology, Delft CN2628, the Netherlands
[d] Railway Engineering Research Institute, China Academy of Railway Sciences Corporation Limited, Beijing 100081, China
[e] Institute of Highway Engineering (ISAC), RWTH Aachen University, Aachen 52074, Germany

ARTICLE INFO

Article history:
Received 14 June 2024
Revised 18 June 2025
Accepted 5 October 2025
Available online xxxx

Keywords:
Ballastless track
Full-section asphalt concrete waterproof layer
Vehicle–track coupling dynamics
Dynamic response
Fractional-order constitutive model

ABSTRACT

The full-section asphalt concrete waterproof layer (FACWL) has garnered significant attention for its outstanding ability to reduce frost heave and thaw-related weakening in railway track beds, particularly in seasonally frozen regions. To explore the dynamic properties of the FACWL, a fractional-order constitutive model was utilized to characterize the viscoelastic behavior of asphalt concrete. Additionally, a vehicle–track coupled finite element (FE) model and the numerical approach incorporating the fractional-order constitutive model were developed and validated via experimental and field testing. Simulation results indicate that applying the FACWL reduces the vertical dynamic response of each structural layer, vertical peak accelerations across the subgrade surface layer exhibited reductions exceeding 30% in both positive and negative directions. Moreover, the tensile strain at the bottom of the FACWL remained relatively low, less than 100 με. Compared with conventional waterproof sealing layers, the viscoelastic nature of the FACWL facilitates energy dissipation, effectively decreasing the overall vibrational amplitude and vertical deformation within the track structure by more than 20%. Consequently, the FACWL plays a crucial role in ensuring the long-term stability of the subgrade and minimizing vibrations in the track system.

1. Introduction

In seasonally frozen regions, water infiltration into a ballastless trackbed can cause freeze–thaw damage, compromising track durability. Waterproof layers are widely utilized to prevent water ingress [1]. Additionally, in some sections, these layers help reduce vertical stress, support the upper structure, and maintain track smoothness [2–5]. Compared with traditional cement concrete waterproof layers (CCWLs), asphalt concrete waterproof layers (ACWLs) offer superior flexibility, crack resistance, and temperature adaptability, making them more suitable for use in China's high-speed railways [6,7]. Typically, ACWL is applied to specific sections such as track shoulders and inter-track zones; however, these applications often result in structural discontinuity and complicate construction [8,9]. To address these challenges, a full-section asphalt concrete waterproof layer (FACWL) has been proposed, which integrates waterproofing and load-bearing functions across the entire track cross-section [10].

FACWL has demonstrated exceptional structural integrity and performance in long-term monitoring, as shown in engineering projects like the Zhengzhou–Xuzhou (Zhen–Xu) high-speed railway [4]. It simultaneously provides water insulation and mechanical support, significantly reducing structural cracking, slab dislocation, and vibrations [11,12]. Nevertheless, FACWL design methods remain predominantly empirical. Current models oversimplify the dynamic wheel–rail interaction by using static circular loads and lack systematic approaches to incorporate temperature effects. This results in inconsistent assumptions about boundary conditions and load transfer mechanisms, limiting their applicability in high-speed rail designs [4,9,13].

* Corresponding authors.
E-mail addresses: hhhwei2005@126.com (W. Huang), chenxh@seu.edu.cn (X. Chen).

https://doi.org/10.1016/j.eng.2025.10.001

Please cite this article as: G. Xu, Y. Wu, W. Huang et al., Dynamic Response of Full-Section Asphalt Concrete Waterproof Layer on Ballastless Tracks Employing Fractional-Order Modeling, Engineering, https://doi.org/10.1016/j.eng.2025.10.001

Although asphalt mixture design methods are well-developed and typically use the dynamic modulus as a performance index, structural design approaches for ACWL and FACWL are still insufficient. Fatigue performance is usually evaluated under idealized stress conditions with static train tests, which do not accurately reflect the real behavior of moving trains. Current design methods fail to correlate field-measured dynamic responses with asphalt fatigue life, leading to structural designs that lack performance-based criteria [14–16].

To achieve more realistic simulations, some studies have employed three-dimensional (3D) finite element (FE) models of vehicle–track interaction (VTI) systems. However, these methods are often limited by the computational cost and complexity of contact modeling. VTI dynamics offer a more efficient and realistic approach by incorporating track irregularities and dynamic load transfer [4,17–19]. Nevertheless, few studies have integrated these models with the FACWL structure, especially to capture realistic wheel–rail interactions [20].

Another significant challenge is the constitutive modeling of asphalt mixtures, whose viscoelastic behavior is sensitive to both time and temperature. Conventional models, such as the generalized Maxwell model (GMM), require numerous parameters to fit experimental data and often fail to predict performance over a wide temperature range [8,14,15,21]. By contrast, the fractional-order viscoelastic model, specifically the two springs, two parabolic elements, and one dashpot (2S2P1D) model, offers more accurate predictions across scales with fewer parameters [22–25]. Although applied in road engineering, its integration with track system modeling, particularly in FE software like ABAQUS (Dassault Systèmes, France), remains scarce [26,27].

This study aims to bridge these gaps by integrating a fractional-order constitutive model with a refined FE VTI model to examine the dynamic response of the FACWL. The influence of the asphalt concrete layer on the dynamic behavior of the overlying track structure and the subgrade is thoroughly examined. Furthermore, the effects of various structural and material parameters on the dynamic response are investigated. This methodology provides a practical and efficient framework for modeling FACWL in ballastless tracks, offering valuable insights for structural design, material selection, and long-term performance evaluation.

Initially, dynamic modulus and fatigue tests are conducted on FACWL samples from the Zheng–Xu test section to characterize their mechanical behavior. A fractional-order model was calibrated using experimental data, and a numerical algorithm was developed for implementation within ABAQUS via user subroutines. Subsequently, a 3D VTI model was constructed, integrating realistic wheel–rail interactions, damping, and boundary conditions. The model accuracy was validated by comparing it with experimental results and theoretical solutions. The dynamic response of the FACWL was then analyzed under various operating conditions, including changes in axle load, speed, temperature, material modulus, and structural thickness. Additionally, the performance of the FACWL was compared to conventional waterproof layer configurations to assess its benefits in vibration mitigation and fatigue resistance.

2. Experiment program

A series of experiments were conducted to characterize the fundamental mechanical properties of the asphalt mixtures used in FACWL. Subsequently, dynamic modulus tests were performed to demonstrate the application of dynamic modulus under high-speed train loading conditions. Details of these tests are provided in Section S1 in Appendix A.

3. Model development

The viscoelastic properties of asphalt concrete are described using the GMM [28,29]. The effectiveness of the model in numerical simulations was enhanced via parameterization with the Prony series [30]. However, increasing simulation precision often necessitates additional Prony series terms, which can reduce computational efficiency. To balance accuracy and efficiency, this section explores the application of a fractional-order constitutive model for asphalt concrete within numerical simulations, exemplified by the FE software ABAQUS. A vehicle–track coupling model incorporating a fractional-order model was developed to analyze the dynamic response of the FACWL, thereby enhancing the understanding and predictive accuracy of simulations under dynamic loading.

3.1. Numerical implementation of the fractional-order constitutive model

This study established a framework for integrating a fractional-order constitutive model for asphalt mixture into FE models through three steps: ① discretizing the continuous relaxation spectrum for FE compatibility, ② implementing the model into FE software (e.g., ABAQUS via user subroutines), and ③ conducting parallel parameter calibration using experimental data. The research compared the GMM, generalized fractional Maxwell (GFM) models, and 2S2P1D models, ultimately selecting GFM-2 and 2S2P1D for subsequent analysis. Corresponding subroutines were developed according to the guidelines in Section S2 in Appendix A.

3.2. Development of vehicle–track coupling model

Extensive studies have shown that the vehicle–track coupling model accurately characterizes the dynamic response of track structures [17,31–33]. In this study, a vehicle–track coupling model incorporating FACWL was established for application in the Zheng–Xu high-speed railway. Fig. 1 presents a schematic of the track and vehicle models.

The Rayleigh damping coefficient defines the structural damping characteristics. Initially, modal analysis was performed based on Rayleigh damping definitions to obtain the first two self-oscillating modes [34]. Fig. 1(a) illustrates the track structure cross-section, featuring a 0.1 m thick FACWL layer that replaces a portion of traditional gravel, distinguishing it from conventional ballastless tracks. Most components are simulated using C3D8R elements, except for Cartesian fasteners spaced at 0.63 m intervals. The dynamic stiffness of the fasteners is set to 1.5 times their static values. The expansion joints for the track plate and base plate are 70 mm and 20 mm wide, respectively. Beam elements represent the base plate transfer bars (Fig. 1(b)). Material parameters are provided in Table 1, with subroutines modeling the viscoelastic behavior of FACWL asphalt. The CRH380-based vehicle model (Fig. 1(c)) comprises a body, bogies, wheelsets, and suspensions. Wheelsets have multiple degrees of freedom (DOFs)—specifically vertical, transverse, roll, yaw, and pitch—resulting in a total of 31 DOFs for the entire vehicle, as detailed in Table 2 [35].

In addition to material and structural configurations, Hertz contact models the interaction between the wheel and rail [36], and a penalty contact simulates interactions among other track structure components [37]. Furthermore, track irregularities based on power spectral density (PSD) are incorporated into the model [17,36]. Infinite boundary elements (CIN3D8) are used to mitigate the adverse effects of stress waves; detailed configuration methods are described in Ref. [38].

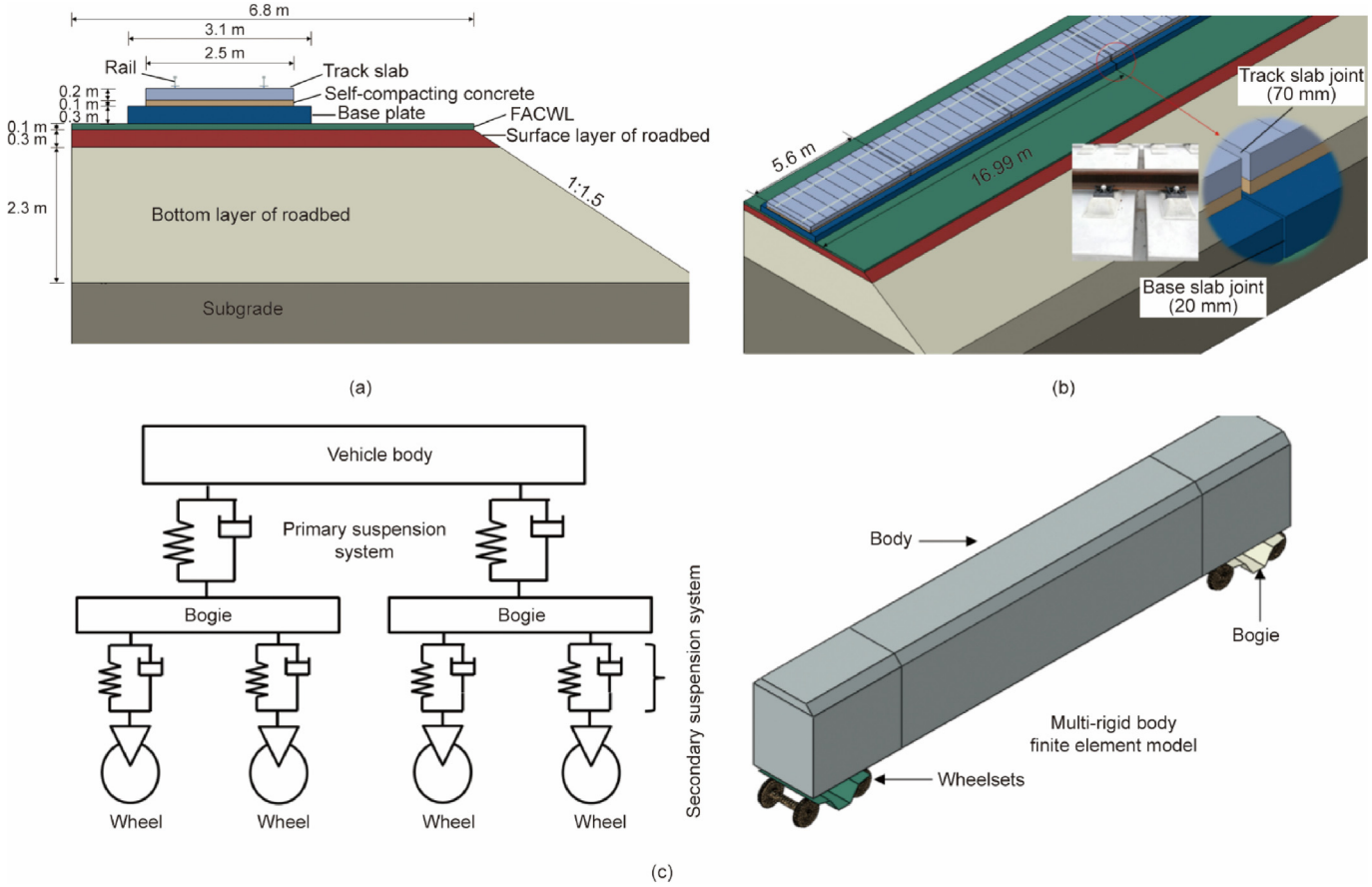

Fig. 1. Schematic of the vehicle–track coupling model. (a) Typical section, (b) overview of the model, (c) vehicle model.

Table 1
Parameters of track structure.

Part	Modulus (MPa)	Poisson's ratio	Density (kg·m^{-3})	Damping ratio
Rail	210 000	0.30	7 800	0.010
Track slab	36 000	0.20	2 500	0.030
Self-compacting concrete layer	32 500	0.20	2 500	0.030
Base slab	32 500	0.20	2 500	0.030
Graded gravel on the surface of the subgrade	220	0.30	2 000	0.045
Bottom of the subgrade	130	0.25	1 800	0.039
Embankment below subgrade	80	0.25	1 700	0.035

Table 2
Vehicle model parameters of CRH380 [35].

Parameter	Unit	Values
Body/bogie/wheelsets mass	kg	40 000/3 200/2 400
Body nodding/shaking/side-rolling inertia	× 10^5 kg·m^2	2.70/2.70/1.15
Bogie nodding/ shaking/side-rolling inertia	kg·m^2	7 200/6 800/3 200
Wheelsets shaking/side-rolling inertia	kg·m^2	1 200/1 200
Vertical/longitudinal/transverse stiffness of primary suspensions	kN·m^{-1}	1 040/9 000/3 000
Vertical/longitudinal/transverse damping of primary suspensions	kN·s·m^{-1}	40/0/0
Vertical/longitudinal/transverse stiffness of secondary suspensions	kN·m^{-1}	400/240/240
Vertical/longitudinal/transverse damping of secondary suspensions	kN·s·m^{-1}	60/500/30
Vehicle spacing	m	17.375
The wheelbase of the bogie	m	2.5
Rolling radius of the vehicle	m	0.46

3.3. Model validation

Validation involved three steps: a user subroutine, constitutive model, and vehicle–track coupling model. Initially, the subroutine was validated by comparing numerical, analytical, and experimental results. Second, the constitutive model was validated by comparing virtual dynamic modulus simulations with experimental data. The third section validates the vehicle–track coupling model by comparing numerical results with field test data. Validations for the first two steps are detailed in Section S3 in Appendix A, respectively. Only the VTI model validation is presented here.

ield test data from the Zheng–Xu high-speed railway confirmed the validity and accuracy of the vehicle–track coupling model. The monitoring points were positioned at the base slab (BS) centerline and structural joints (Fig. 2(a)). For an FACWL thickness of 10 cm and a train speed of 250 km·h^{-1}, Figs. 2(b)–(d) show three dynamic response parameter curves. The test results demonstrated two vertical displacement peaks on the track surfaces from wheelset superposition under single-train loads. The measured vertical displacement

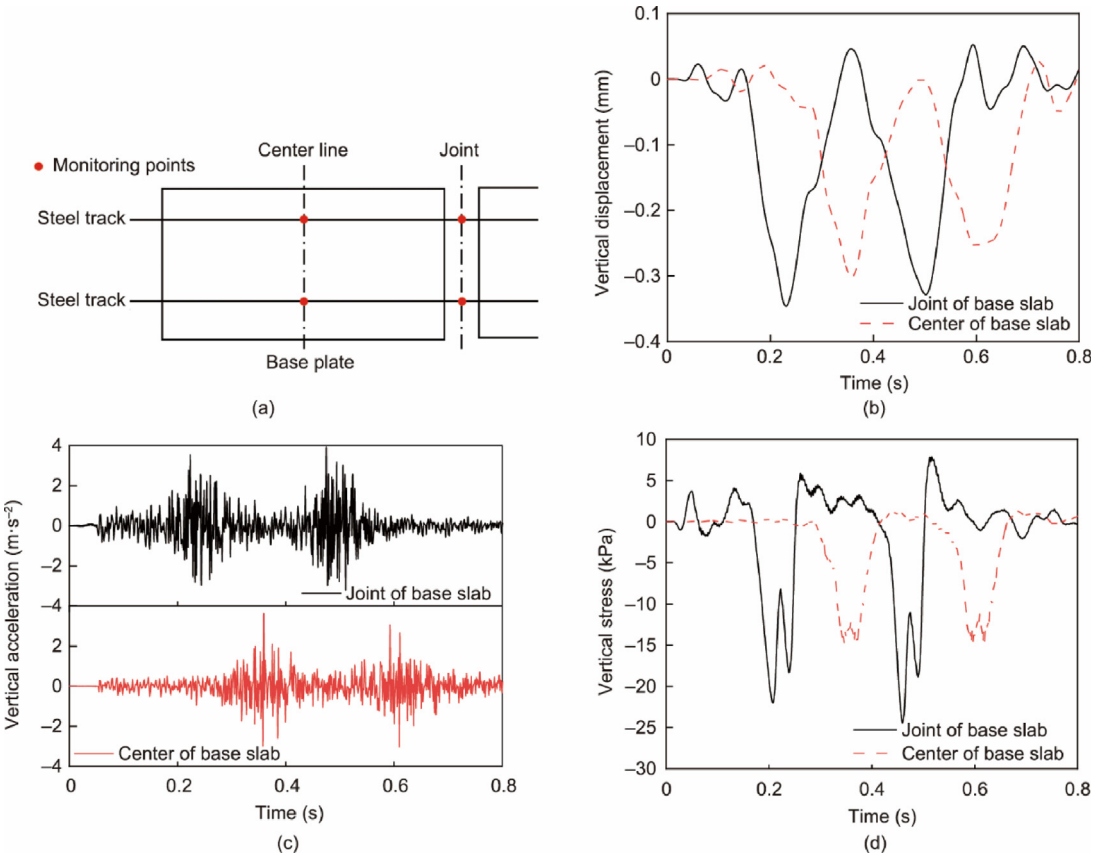

Fig. 2. Process of validating vehicle–track coupling model. (a) Monitoring section, (b) vertical displacement, (c) vertical acceleration, (d) vertical stress.

ranged from 0.01 to 0.5 mm, and vertical acceleration ranged from 1.6 to 3.2 $m \cdot s^{-2}$. The FE model predictions aligned with field measurements for vertical displacement and acceleration; however, minor peak deviations may have resulted from variations in the track irregularity spectrum. The validated model effectively captured the track structure dynamics under train loads, permitting an accurate FACWL dynamic response analysis.

4. Simulation results

4.1. Unfavorable load location analysis

4.1.1. Longitudinal distribution

To analyze the dynamic response of the FACWL, the unfavorable longitudinal train load position that causes the largest response must be identified. As shown in Fig. 3, three load conditions (Conditions (1), 2, and 3) were focused on the rear wheels of the front bogie: at the BS end joints, track slab (TS) joints, and BS center.

At an ambient temperature of 20 °C and a train speed of 350 $km \cdot h^{-1}$, a vehicle–track coupling model calculated vertical stress, displacement, acceleration, and base tensile strain in FACWL under various conditions (Table 3). Dynamic responses under Conditions 1, 2, and 3 indicated heightened structural vulnerability when wheelsets aligned with track cracks, especially base-slab end cracks. Table 3 shows an increased risk of transverse cracking, as longitudinal tensile strain significantly exceeds transverse strain at the FACWL base. Fig. 4 depicts transverse strain concentration near the loaded BS edges and longitudinal strain accumulation at structural joints under Condition 1, necessitating design adjustments. Notably, the tensile strain of asphalt concrete under train loads remained low (1/5–1/10 of conventional pavements), highlighting the superior fatigue resistance of FACWL. Enhancing the fatigue limit of the asphalt mixture effectively mitigates flexural cracking during service.

4.1.2. Spatial distribution

Fig. 5 illustrates the transverse distribution of the dynamic response of FACWL under load Condition 1. The dual-line routes extend from 0 m to the shoulder boundary at 6.8 m. Vertical displacement (Fig. 5(a)) exhibited minimal variation between the

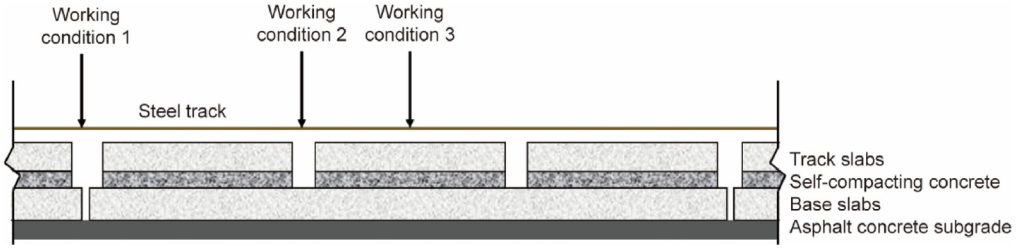

Fig. 3. Location of the selected load conditions.

Table 3
Dynamic response of FACWL under different working conditions.

Dynamic response	Working condition		
	1	2	3
Vertical stress (kPa)	36.18	27.15	19.21
Vertical displacement (mm)	0.39	0.37	0.30
Vertical acceleration ($m{\cdot}s^{-2}$)	4.95/ −4.32	4.41/ −4.54	4.31/ −3.47
Longitudinal tensile strain at the bottom of the layer (με)	7.01	20.57	13.94
Transverse tensile strain at the bottom of the layer (με)	7.01	6.13	4.88

top and bottom layers of FACWL, peaking below the track near the shoulder. Fig. 5(b) indicates higher vertical stress at the FACWL base, peaking near the slab edge. Fig. 5(c) reveals predominant transverse compression at the FACWL top, with minimal transverse tensile strain concentrated beneath the track at the base. Fig. 5(d) illustrates the longitudinal tension on both surfaces, with higher intensity at the bottom and peak values near the slab center. The dynamic response is primarily concentrated beneath the track and at the slab edges, significantly influencing the base width of the slab.

The positions beneath the rail and at the BS edges on the shoulder were selected to plot vertical surface stress and bottom longitudinal strain distribution curves along the track, demonstrating the transverse distribution of the dynamic behavior of FACWL (Fig. 6). The structural joints of the foundation slab are depicted by two vertical lines in Fig. 6.

Longitudinal distribution data in Fig. 6 reveal two peaks in bottom surface longitudinal strain and FACWL vertical stress along the length of the track. Peak concentrations occur at foundation slab expansion joints, spanning approximately 10 m longitudinally. Field data from Jing–Hu high-speed railway tests show subgrade surface (SS) dynamic stress variations within a 9–10 m longitudinal range, consistent with simulations. Base slab edges are more critical for vertical stresses, whereas track-aligned positions exhibit greater susceptibility to longitudinal tensile strain [39].

Fig. 7 presents the longitudinal distributions of draped displacements and stresses (strains) within the graded gravel layer. Similar to FACWL, the dynamic response index of the graded gravel layer peaks in the joint areas of the BS structure.

In conclusion, the spatial distribution of the dynamic response revealed stress–strain concentrations likely occurring in the FACWL near the structural joints of the BS. This region is a vulnerable area susceptible to damage over its service life; therefore, it must be prioritized in structural design to mitigate potential risks.

4.1.3. Selection of dynamic response parameters

The distribution indicates that when train loads are applied to the base plate end, the highest dynamic responses are observed in the bed FACWL and the adjacent graded gravel layer near the structural joints. Within the bed FACWL, fatigue cracking emerges as the primary potential damage under train loads. Drawing on highway asphalt pavement design principles, the longitudinal bending/tensile strain at the bottom layer was used as the main control index, whereas vertical displacement at the top reflected overall subgrade stiffness. In the graded gravel layer, vertical compressive stress (strain) on the top surface dictates permanent deformation owing to modulus differences with asphalt concrete. The locations of the dynamic response indicators are shown in Fig. 8.

4.2. Influence factors of dynamic response

To clarify the mechanical properties of FACWL, the study investigated the effects of axle load (140 kN), speed (350 $km{\cdot}h^{-1}$), FACWL thickness (10 cm), temperature (20 °C), and graded gravel modulus (220 MPa) on SS dynamics. Sensitivity analysis was performed by individually varying each parameter under standard operating conditions.

4.2.1. Vehicle axle weight

Currently, China railway high-speed (CRH) trains operate on ballastless rail lines in China, with bogie axle weights typically ranging from 14 to 18 t. In anticipation of potential increases in train axle loads for future passenger transportation, the axle load range was expanded to five levels: 100, 140, 180, 220, and 260 kN. This study examined the impact of train axle load on the dynamic response parameters of the bed surface, as displayed in Fig. 9.

The Fig. 9(a) demonstrates that train axle load significantly influences each dynamic response indicator of the SS, with a linear increase corresponding to the axle load. Specifically, for each additional 1 t axle weight, the SS dynamic responses are as follows: 0.028 mm vertical displacement of the FACWL, 1.7 με maximum

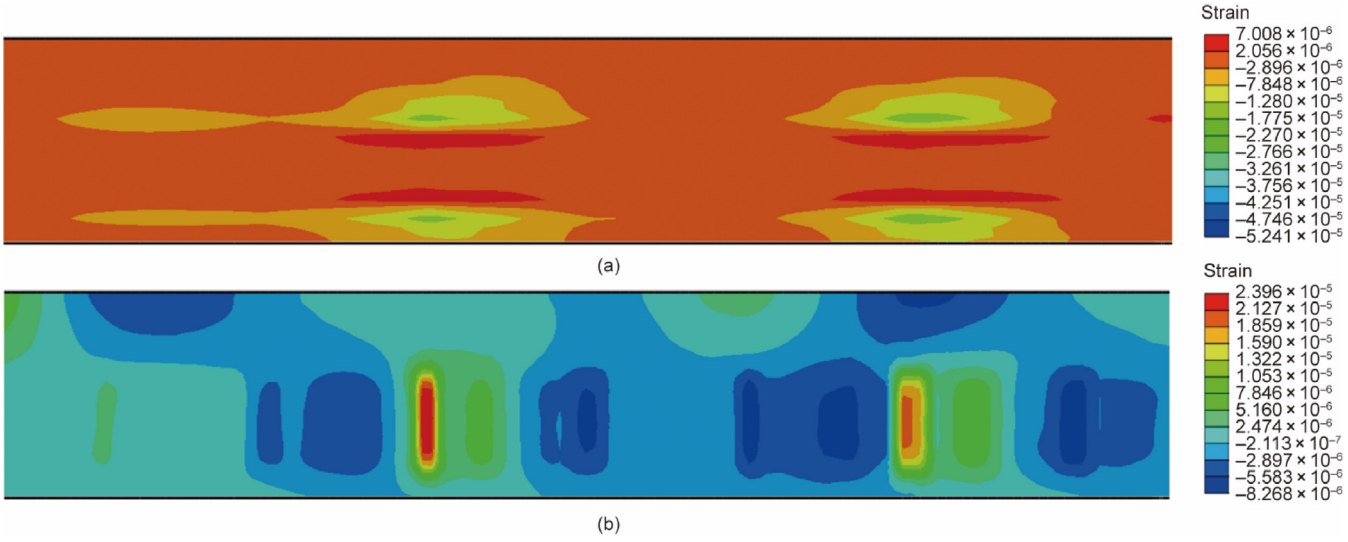

Fig. 4. Strain clouds at the bottom of FACWL. (a) Transverse strain, (b) longitudinal strain.

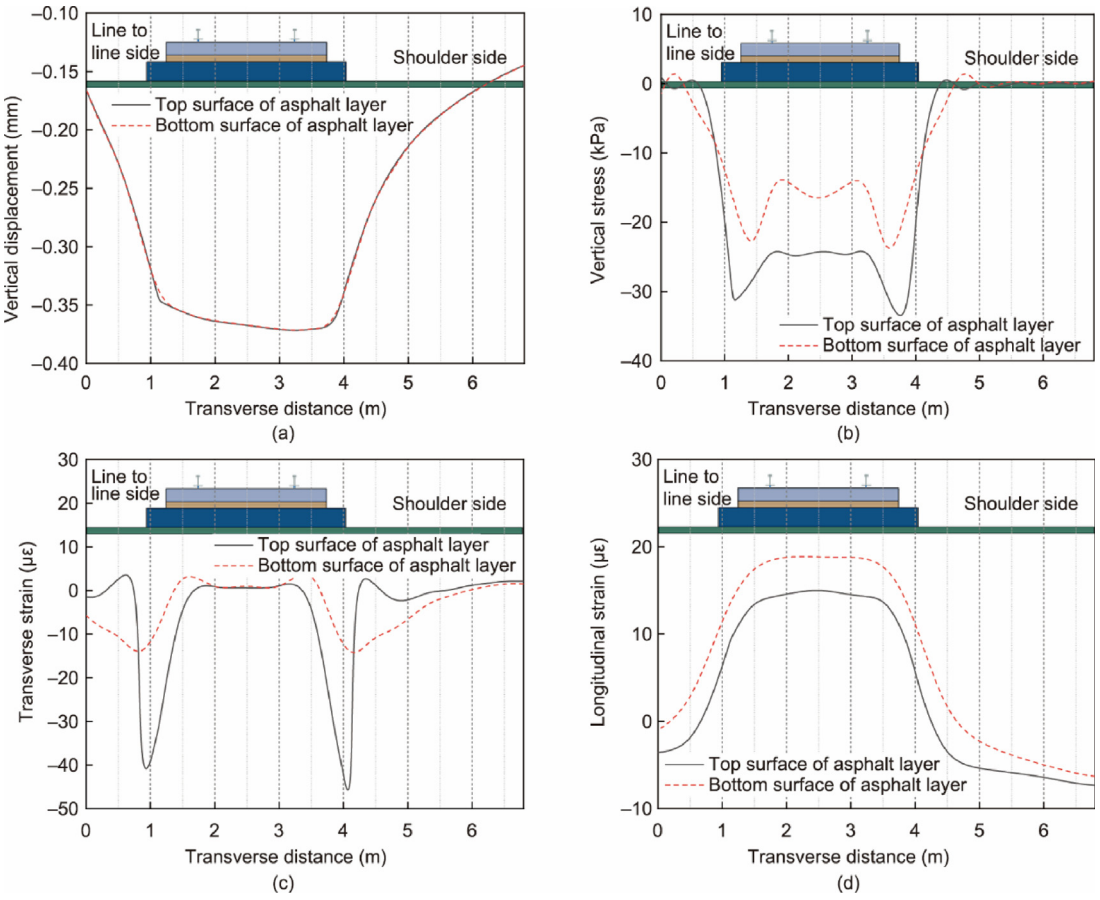

Fig. 5. Transverse distribution of dynamic response of FACWL. (a) Vertical displacement, (b) vertical stress, (c) transverse tensile strain, (d) longitudinal tensile strain.

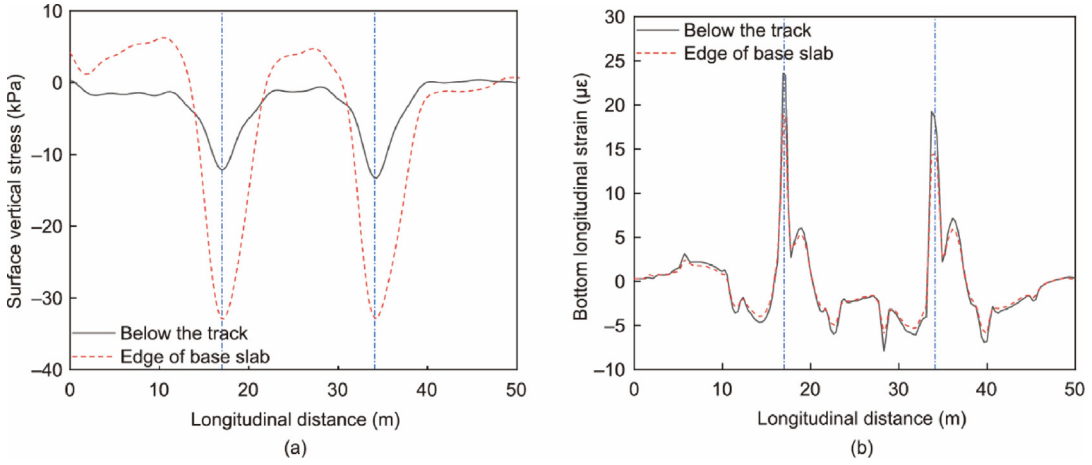

Fig. 6. Longitudinal distribution of dynamic response of FACWL. (a) Vertical stress at the surface, (b) longitudinal strain on the bottom of the surface layer.

tensile strain at the FACWL base, 1.06 kPa vertical stress, and 4.32 με vertical strain in the graded gravel layer. When the train axle load increases from 140 to 180 kN, each dynamic response indicator of the SS rises by approximately 27%.

According to China's high-speed railway design code, dynamic stresses on the SS are influenced by train speed, axle load, vehicle dynamics, track structure, track irregularities, and subgrade conditions. Train axle load and speed have the most significant effects. The empirical equation (Eq. (1)), applicable for calculating the amplitude of dynamic stress (σ_{dl}) on the SS, is as follows:

$$\sigma_{dl} = k \times P \times (1 + \alpha v) \quad (1)$$

where the coefficient is denoted as k = 0.26. α is an empirical constant that varies with speed and takes the value 0.003 when the speed ranges from 300–350 km·h^{-1} and 0.004 across 200–250 km·h^{-1}. P (kN) represents the static axle load on the train, v (km·h^{-1}) is the train speed, while $1 + \alpha v$ represents the impact coefficient, and the maximum impact coefficient for passenger railways is 1.9.

The vertical stress results depicted in Fig. 9(b) were regressed using the aforementioned equation. Eq. (2) provides an

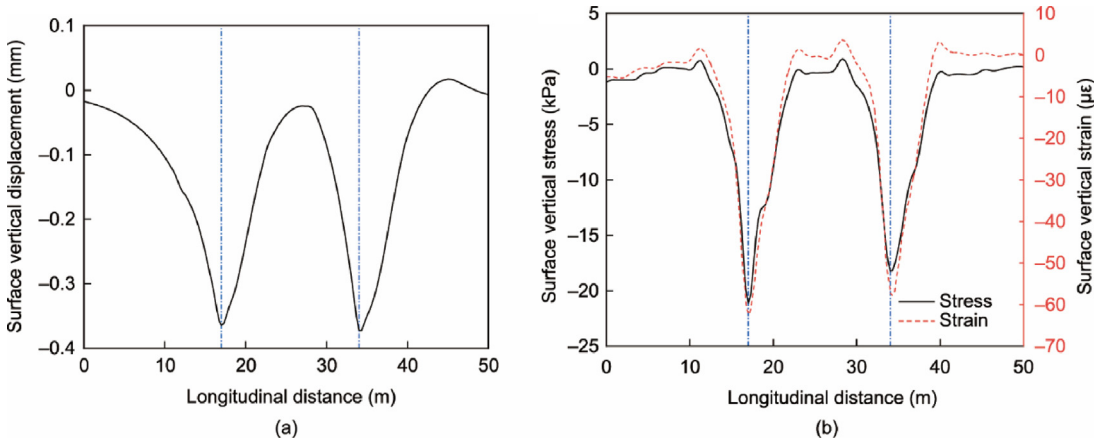

Fig. 7. Longitudinal distribution of the dynamic response of the graded gravel layer in the subgrade. (a) Surface vertical displacement, (b) surface vertical stress and strain.

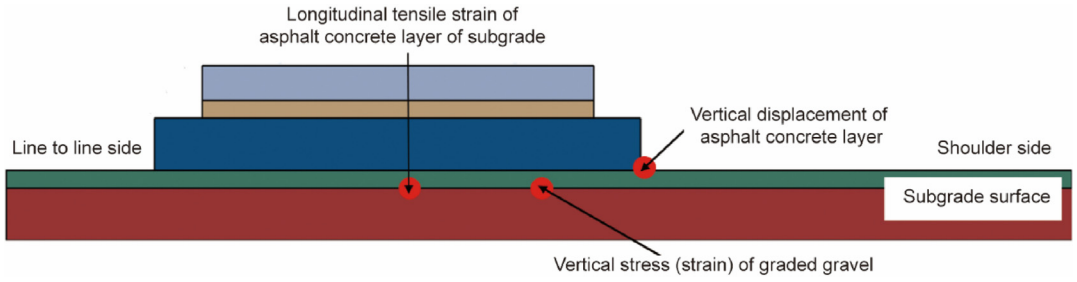

Fig. 8. Data collection position of dynamic response.

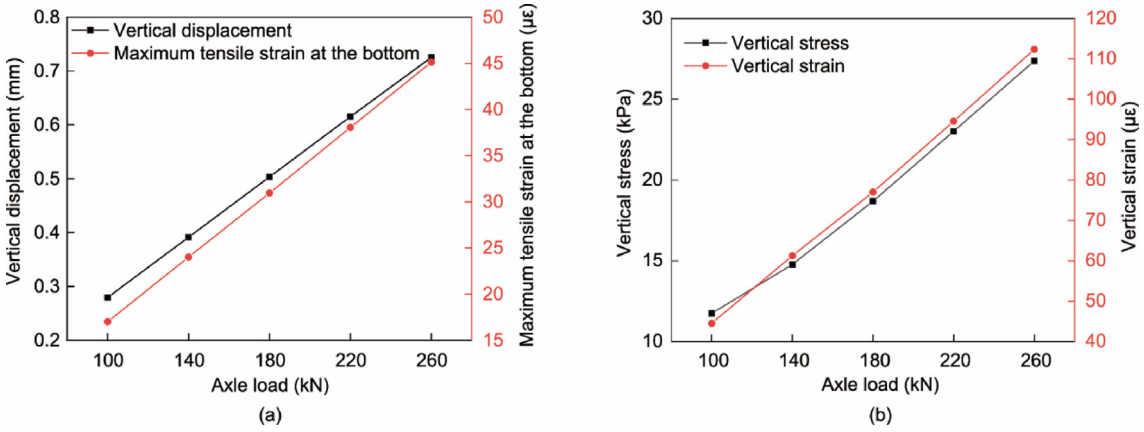

Fig. 9. Effect of train axle load on the dynamic response of the SS. (a) FACWL, (b) graded gravel layer.

approximate formulation of the vertical tension at the top of the graded gravel SS layer under various axial loads at 350 km·h^{-1}:

$$\sigma_{dl} = 0.0556 \times P \times (1 + \alpha v) \quad (2)$$

The attenuation curve of vertical dynamic stress with depth in the subgrade under various axial pressures is illustrated in Fig. 10. The top surface of the graded gravel layer serves as the reference depth. As the axle load increased, the vertical strains at each subgrade depth also increased. Between 0 and 2 m, vertical stress degradation was most pronounced. Below 2 m, vertical tension did not vary significantly.

The attenuation curve of dynamic stress in the roadbed can be approximated using Eq. (3):

$$\eta = 1 - \frac{z}{a + b \cdot z} \quad (3)$$

where η represents the attenuation coefficient of dynamic stress, defined as the ratio of the dynamic stress at a specific depth to the dynamic stress at the surface, z represents the soil depth in the subgrade, and a and b are curve-fitting coefficients.

The fitting results of the attenuation curves for different axle loads are summarized in Table 4. The analysis revealed that axle load did not influence the coefficient of the attenuation curve, indicating that variations in axle load did not influence the dynamic stress trend in the attenuation trend of the subgrade.

4.2.2. Vehicle speed

All new Chinese high-speed rail lines operate at design speeds exceeding 250 km·h^{-1} and upgraded existing lines operate above 200 km·h^{-1}. This section investigates the impact of train speeds (200–400 km·h^{-1}) on track surface dynamics using data from

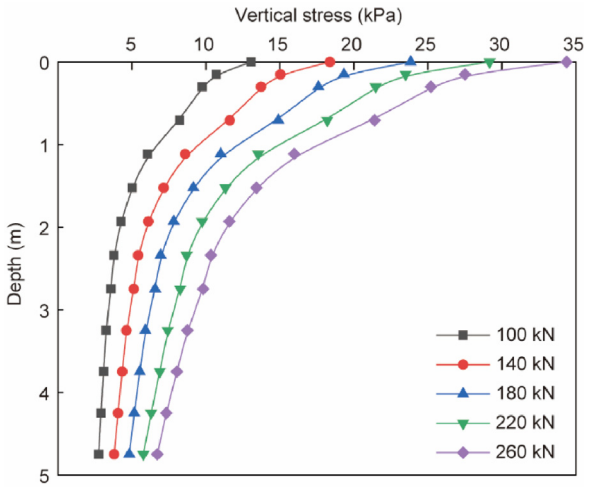

Fig. 10. Distribution of dynamic stress along depth in subgrade under different train axle loads.

Table 4
Fitting results of dynamic stress attenuation curves of subgrade under different axial loads.

Axle load (kN)	Curve-fitting coefficient		Coefficient of determination
	a	*b*	R^2
100	0.899	1.061	0.9926
140	0.915	1.058	0.9931
180	0.886	1.06	0.9928
220	0.887	1.066	0.9925
260	0.884	1.067	0.9919

Fig. 11. Increasing the speed from 200 to 400 km·h^{-1} led to a 1.3% increase in FACWL base vertical displacement and 2.4% increase in longitudinal tensile strain (Fig. 11(a)). By contrast, the vertical stress and strain of the graded gravel layer increased by 4.9% and 5.6%, respectively. Subgrade surface dynamics showed minimal sensitivity to speed changes. The viscoelastic properties of FACWL reduce the impact of speed compared with gravel layers. Fig. 11(b) shows the vertical stress variations derived from Eq. (3), which correspond with the simulation results.

Fig. 12(a) presents the time-history curves for longitudinal strain at the FACWL base for various train speeds. Evidently, the peak longitudinal strain response from each wheel load was not significantly pronounced, suggesting that individual bogies primarily controlled the peak longitudinal strain of FACWL.

To elucidate the frequency response characteristics of the FACWL under the stress of moving trains, the longitudinal strain time-history curve was subjected to a rapid Fourier transformation. The resulting spectral curves are presented in Fig. 12(b). The spectrum reveals four characteristic peaks within the 0–20 Hz range. Notably, the second peak exhibited the highest strain amplitude, predominantly governing the longitudinal strain response. The characteristic frequency were determined using Eq. (4).

$$f = \frac{v}{L} \tag{4}$$

where f (Hz) is the peak response frequency, L (m) is the disturbance wavelength.

As illustrated in Table 5, the peak frequency of the longitudinal strain response increases with train speed, whereas the characteristic wavelength remains approximately 17 m. This 17 m wavelength corresponds to the fixed distance between the two bogies of a single carriage in the vehicle model, as detailed in Table 5.

Bodin et al. [40] introduced the concept of "equivalent modulus" in asphalt pavement design, substituting viscoelastic FACWL with an equally thick linear elastic layer to match the peak strain at the base of the structural layer. This modulus depends on the speed and temperature conditions of the structural layer, enabling the viscoelastic dynamics to be transformed into elastic responses. In practice, the dynamic modulus at 20 °C and 10 Hz is typically used as the material input for elastic layered systems. Similarly, determining the frequency-specific dynamic modulus enables its use as a material parameter in elastic models for the structural design of subgrade FACWLs.

The peak values in the longitudinal stress and strain time-history curves at the bottom are utilized to determine the dynamic response modulus of the FACWL of subgrade at various train speeds. Referencing the primary dynamic modulus curve at 20 °C facilitates the calculation of dynamic modulus values for various peak frequencies. A comparative analysis was conducted between the dynamic response modulus calculated at different vehicle speeds and actual dynamic modulus measurements in Fig. 13. The dynamic response modulus derived from the FACWL subgrade responses matched the dynamic modulus test results across all speeds. Therefore, the dynamic modulus corresponding to the peak frequency at each train speed serves as the equivalent modulus for the FACWL subgrade.

Fig. 13 shows that the dynamic modulus at a peak frequency of 5.56 Hz and train speed of 350 km·h^{-1} is 3413.4 MPa, which is used as the elastic modulus of FACWL in FE modeling. Fig. 14 compares these results with those from the viscoelastic model, demonstrating a strong correlation in the dynamic response time-history curves of SS layer when using elastic parameters under specific

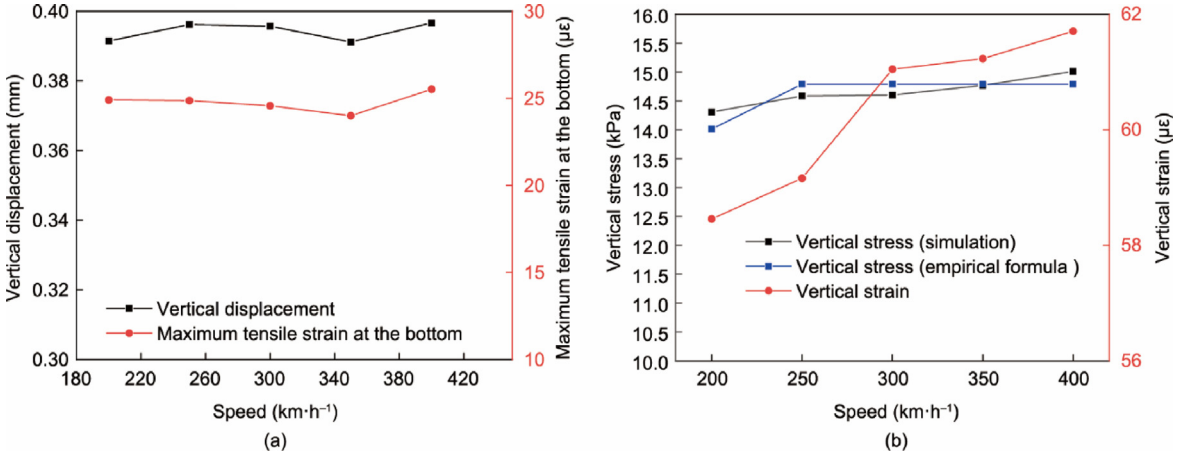

Fig. 11. Influence of train speed on dynamic response of track bed surface layer. (a) FACWL, (b) graded gravel layer.

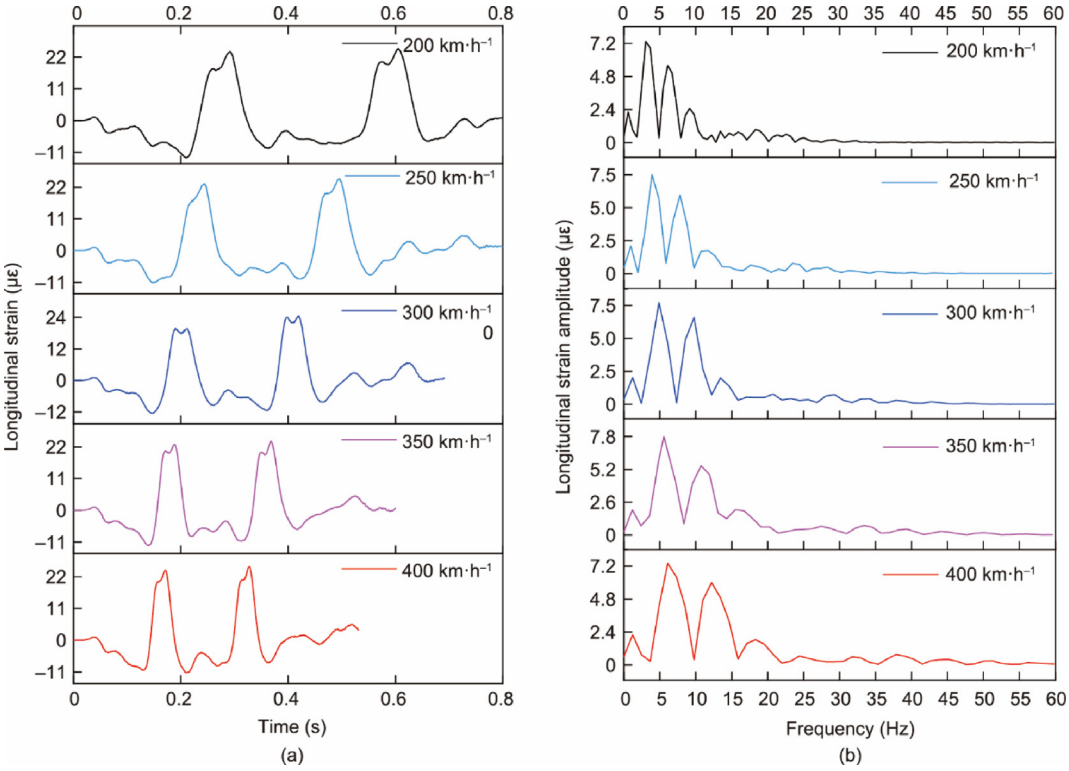

Fig. 12. Time–frequency curves of longitudinal strain of FACWL at different train speeds. (a) Time-history curve, (b) frequency domain spectrum.

Table 5
Peak frequency and characteristic wavelength of longitudinal strain response at different train speed.

Velocity (km·h^{-1})	Peak frequency	Characteristic wavelength
200	3.05	18.20
250	3.91	17.78
300	4.88	17.07
350	5.56	17.48
400	6.10	18.20

conditions. Although most indicators exhibited a relative error of < 5%, the FACWL-based longitudinal stress showed slightly higher peak value deviations. Consequently, the peak frequency dynamic modulus from Table 5 can be adopted as FACWL's elastic model parameter at 20 °C for structural design. Regression analysis established the relationship between peak response frequency and train speed as expressed in Eq. (5).

$$f = \frac{v}{63.5943}, R^2 = 0.9880\# \quad (5)$$

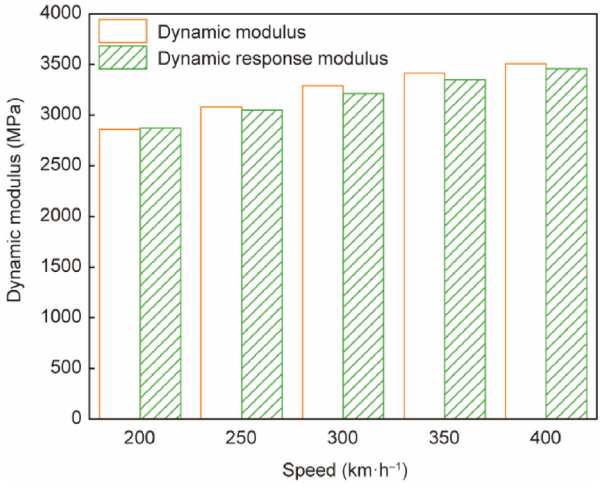

Fig. 13. Comparison of dynamic modulus and dynamic response modulus at different speeds.

4.2.3. Temperature of asphalt concrete

Asphalt concrete, being temperature-sensitive exhibits substantial modulus variations with temperature. In this section, the temperature of FACWL ranges from −30 to 40 °C. The impact of temperature on the dynamic response of the SS layer was investigated, with findings presented in Fig. 15.

Fig. 15(a) illustrates an inverse correlation between the dynamic modulus of the asphalt mixture and temperature: As temperature increases, modulus decreases, resulting in increased vertical displacement and, consequently, the highest tensile strain at the FACWL base. Specifically, when temperature increased from 30 to 40 °C, vertical displacement and maximum longitudinal tensile strain at the FACWL base surged by 19.8% and 200%, respectively, compared with the extreme temperature condition. This underscores that temperature significantly influences the tensile strain at the FACWL base. The curve in the figure mirrors the primary dynamic modulus curve, displaying an "S" shape, which indicates that vertical displacement and bottom tensile strain do not consistently vary with temperature fluctuations. By referencing the instantaneous and long-term equilibrium moduli from the dynamic modulus curve, the upper and lower bounds of the dynamic response index of FACWL relative to temperature variation can be estimated. Additionally, both vertical compressive stress and strain of the graded gravel layer increased with temperature, as depicted in Fig. 15(b). Vertical strain was more sensitive to temperature changes than vertical stress. Temperature

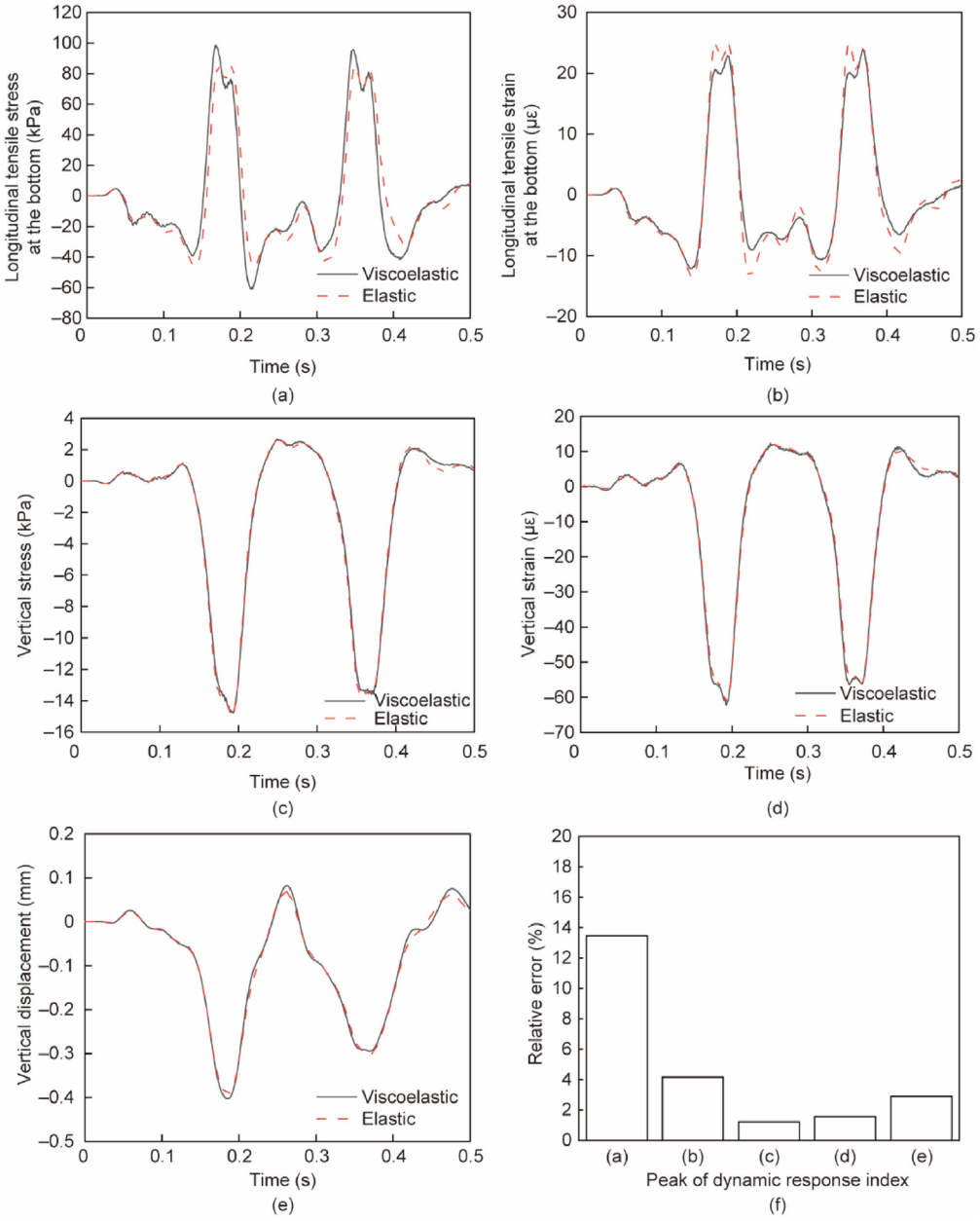

Fig. 14. Comparison of FE calculation results of elastic and viscoelastic models. (a) Longitudinal stress of FACWL, (b) longitudinal strain of FACWL, (c) vertical stress on the top of graded gravel layer, (d) vertical strain on the top of graded gravel layer, (e) vertical displacement on the surface of subgrade, (f) relative errors between elastic and viscoelastic models (corresponding to (a)–(e)).

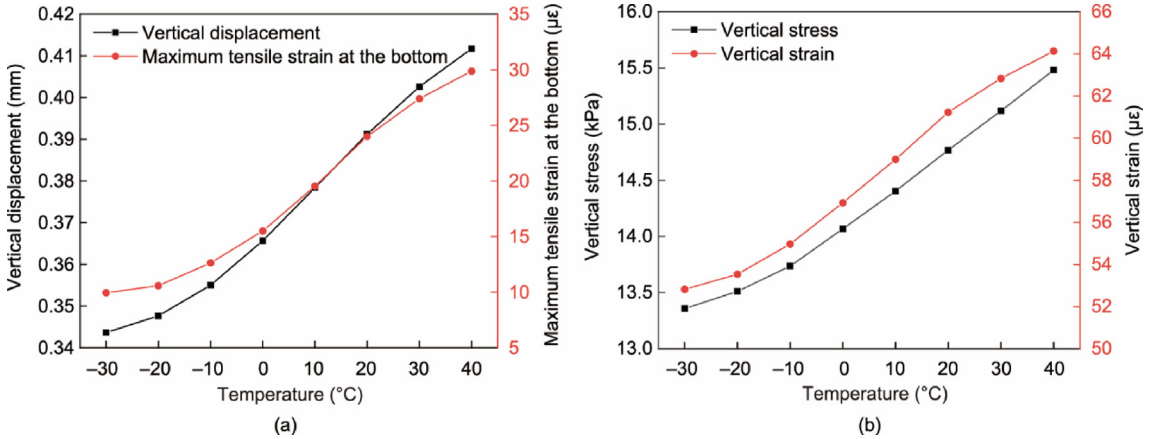

Fig. 15. Influence of FACWL temperature on dynamic response of subbed surface. (a) FACWL, (b) graded gravel layer.

variations in the FACWL were associated with modulus alterations. Asphalt mixtures exhibiting higher modulus at identical temperatures more effectively attenuate dynamic responses to train loads. However, an excessively high modulus can result in brittle failure under low-temperature conditions during rapid temperature drops. The selection of FACWL materials for subgrade construction must balance the impacts of train loads with environmental temperature factors.

Fig. 16 illustrates the spectral curve of longitudinal strain in the asphalt concrete bottom layer across various temperatures. At a constant train speed, the peak frequency position remained consistent across temperatures, although its amplitude increased with rising temperature. This suggests that the peak frequency of FACWL under train load is primarily dependent on train speed and is minimally influenced by temperature. Consequently, Eq. (5) can be employed to calculate the peak frequency of FACWL under varying temperatures owing to train loads.

4.2.4. Combination of subgrade surface thickness

Currently, FACWL is underutilized in subgrade applications. To ensure track elevation consistency, the SS thickness is retained identical to conventional sections, and the ballastless track foundation bed is maintained at 0.4 m. For dense asphalt mixtures, the single-layer compaction thickness must exceed 2.5–3.0 times the maximum nominal size of the aggregate (16 mm in this study). This study examined asphalt mixtures with a minimum compaction thickness of 5 cm and varying FACWL thicknesses (5, 8, 10, 12, and 15 cm) under constant subgrade parameters. The computational results are shown in Fig. 17.

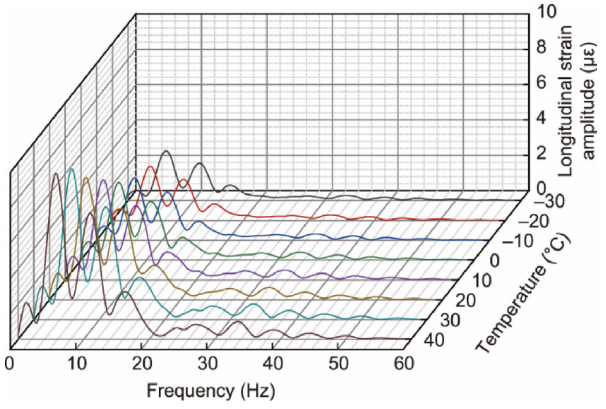

Fig. 16. Spectral curves of longitudinal strain of asphalt concrete at different temperatures.

Fig. 17 illustrates that as the dynamic response of the FACWL decreases with increased layer thickness, the graded gravel layer exhibits the opposite behavior. This occurs because a thicker FACWL reduces the thickness of the graded gravel layer, thereby lowering its overall rigidity. Consequently, vertical stress and strain at the surface are intensified. Notably, the vertical displacement of the FACWL and maximum tensile strain at its base decreased by 8.0% and 8.5%, respectively, when the FACWL thickness was increased from 5 to 20 cm. This suggests that increasing FACWL thickness to mitigate dynamic responses may not be economically viable, as it would significantly raise material costs and require double-layer paving technology, thereby substantially increasing construction expenses. In summary, when the total thickness of the SS is maintained constant, the optimal FACWL thickness should range between 5 and 10 cm.

Subsequently, a second subgrade configuration was examined with variable total surface thickness. Only the graded gravel layer remained constant (20 cm intermediate layer), whereas the FACWL thickness varied. Construction practices indicate that graded gravel should be placed in layers of 15–30 cm with compaction at each stage. Fig. 18 demonstrates that increasing the FACWL thickness linearly reduces the dynamic response in both layers. Additionally, this thickness enhancement decreased the permanent deformation of graded gravel and extended the fatigue life of asphalt concrete.

When designing the surface structure of the foundation bed, integrating the FACWL with the graded gravel layer into a single compacted layer can lower construction costs. To incorporate train load impacts, the FACWL should ideally be 5–10 cm thick, whereas the graded gravel layer should range from 15 to 30 cm. The thickness combination of the concrete structure must be validated using expected service life and fatigue equations to ensure durability and performance.

4.3. Comparison with other ACWL structures

Currently, the SSs of Chinese high-speed railways are predominantly covered with a cement concrete waterproof layer. However, in cold and seasonally freezing regions, this layer often experiences cracking, breaking, chalking, and other degradations, leading to the foundation bed and slurry softening, which compromises high-speed railway safety. Alternatively, the ACWL structure involves placing the asphalt waterproof layer only between the lines and trackbed shoulders, serving primarily as a waterproofing and sealing layer rather than a direct load-bearing component. By contrast, the FACWL is applied across the entire SS, functioning as a waterproof layer that transfers and disperses the upper load. Therefore, these two structural systems need to be comparatively analyzed

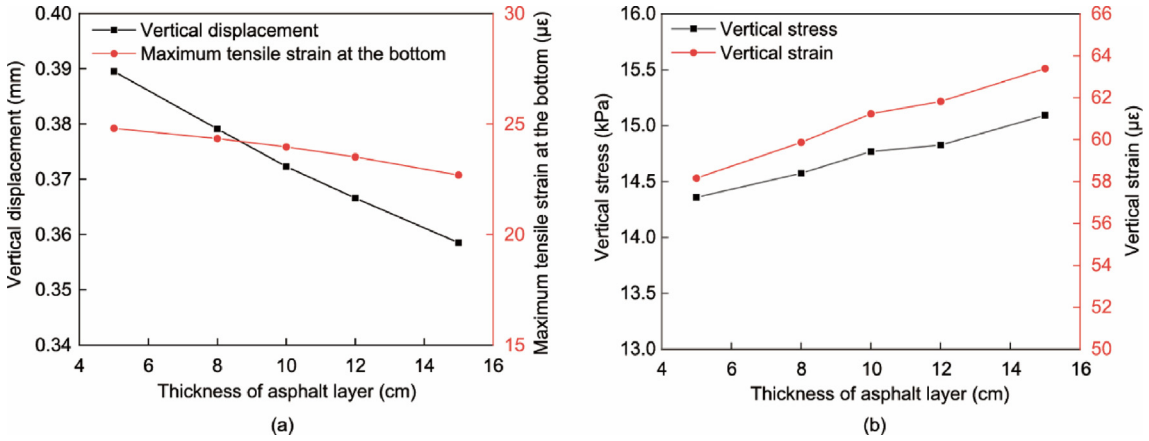

Fig. 17. Influence of FACWL thickness on the dynamic response index of the SS (Plan 1). (a) FACWL, (b) graded gravel layer.

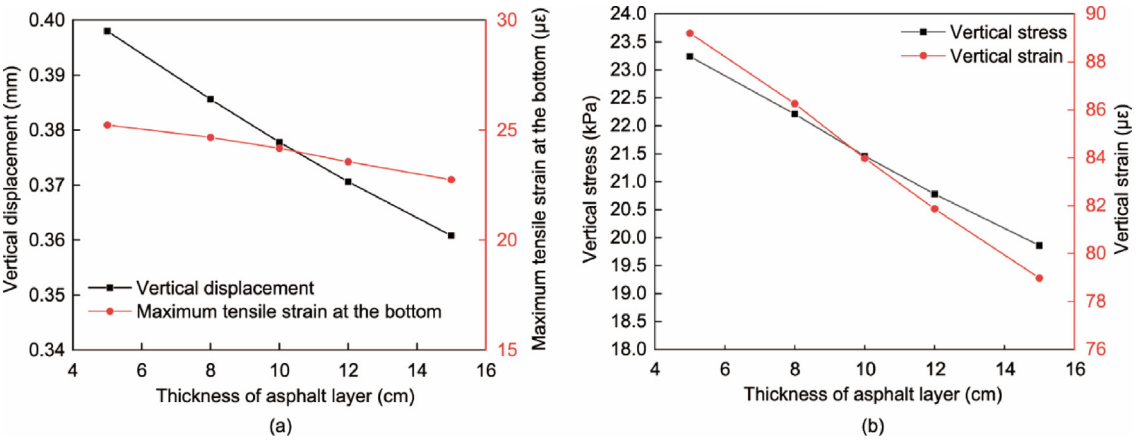

Fig. 18. Influence of FACWL thickness on the dynamic response index of the SS (Plan 2). (a) FACWL, (b) graded gravel layer.

for comprehensively assessing the impact of FACWL on both track and subgrade structures.

In the FE model for traditional cement concrete waterproofing layers, the SS comprised 0.4 m of graded gravel. Conversely, the asphalt concrete waterproofing seal utilized a SS layer consisting of 0.1 m of asphalt concrete and 0.3 m of graded gravel. Fig. 19 compares the dynamic responses of these two configurations at a train speed of 350 km·h^{-1}. Abbreviations used in Fig. 19 include TS, self-compacting concrete (SCC), BS, SS, subgrade bottom (SB), embankment (EB), maximum positive acceleration (MPA), and maximum negative acceleration (MNA).

Fig. 19 demonstrates that applying asphalt concrete reduces vertical peak accelerations across the track and subgrade layers, with the SS layer experiencing over a 30% decrease in both positive and negative accelerations. The FACWL was more effective in mitigating peak acceleration on adjacent bed surfaces and BSs compared with other layers. Fig. 20 displays that the room-temperature modulus of asphalt concrete, which is ten times that of gravel, significantly decreases vertical strain in the SS. Additionally, the FACWL vertical strain exhibits notable hysteresis relative to vertical tension, indicating that the viscous properties of asphalt concrete dissipate kinetic energy from the superstructure as

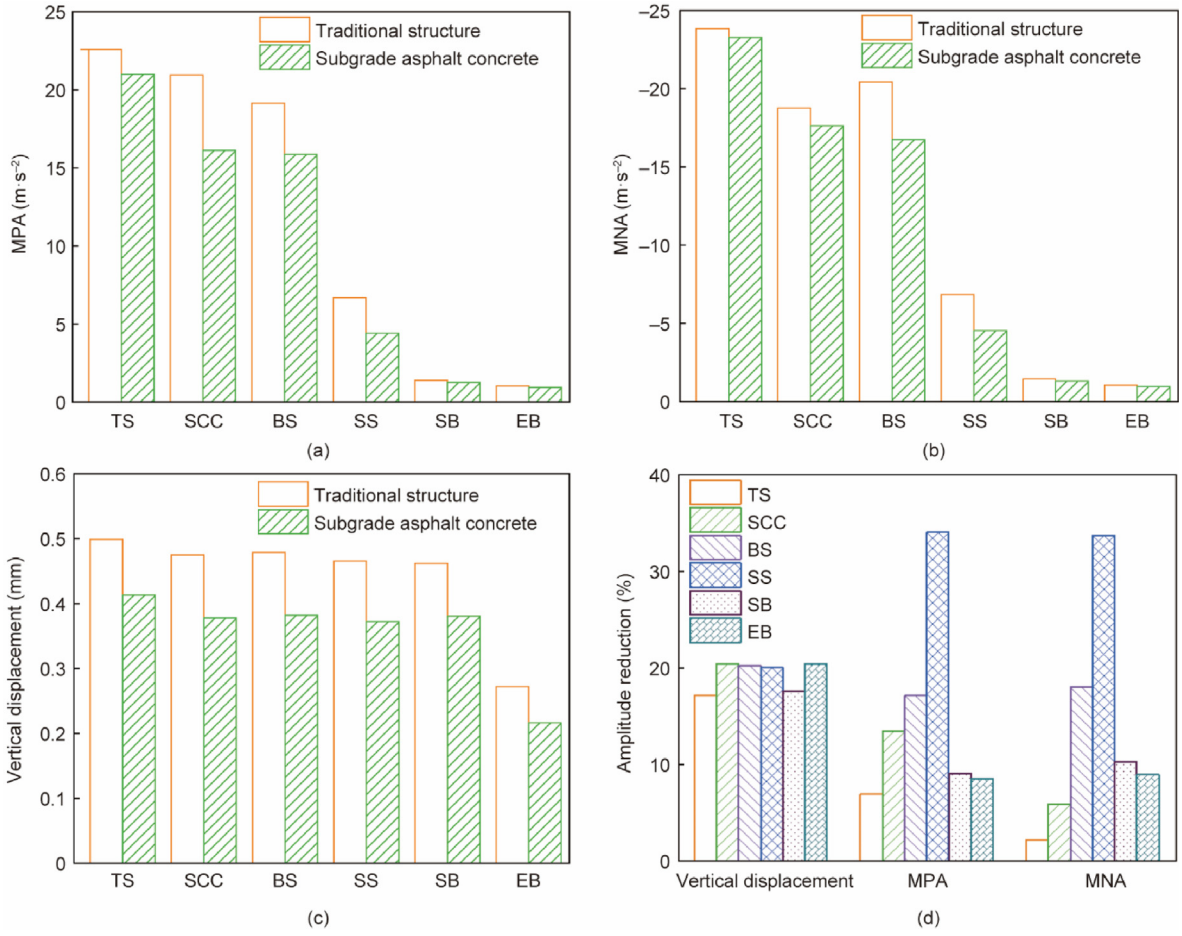

Fig. 19. Comparison of dynamic response peaks between track and subgrade structural layer. (a) MPA, (b) MNA, (c) vertical displacement, (d) decline in dynamic response.

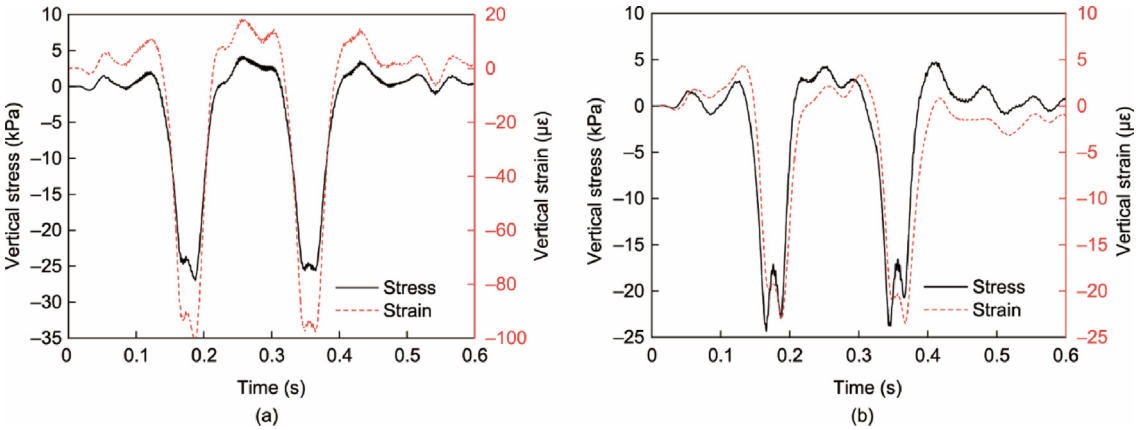

Fig. 20. Time-history curves of vertical stress and strain in the surface layer of the foundation bed. (a) Traditional ACWL, (b) FACWL.

internal energy during vibrations, thereby damping vibrations within the track and subgrade structures.

Typically, the transition in stiffness between the upper rigid construction and lower flexible structure is achieved by installing a full-section asphalt concrete waterproof closure layer on top of a high-speed railway subgrade. This layer mitigates overall vibration and vertical deformation of both the track and subgrade while extending the fatigue life of ballastless tracks and SS layers. Compared with traditional cement concrete, asphalt concrete offers superior advantages for *in-situ* construction, repair, and maintenance, demonstrating significant potential and value as the surface layer for high-speed railway subgrades.

It should be noted that this study assumes a constant dynamic modulus for the asphalt concrete. However, environmental factors, particularly water, can significantly influence the dynamic mechanical properties of asphalt concrete. The effect of freeze–thaw cycles on the dynamic modulus of asphalt mixtures should be further investigated through laboratory testing, in order to elucidate the long-term evolution of the dynamic mechanical behavior of asphalt concrete layers in subgrade under freeze–thaw damage. Morover, the car body, bogie, and wheel set are all treated as rigid bodies, with their elastic deformation during motion neglected. The relative motion between these components is constrained by either elastic or rigid connections—a simplification that significantly deviates from real-world behavior.

5. Conclusions

To accurately analyze the dynamic response of FACWL, this study initially investigated the mechanical properties of asphalt materials and developed a discretization method for the fractional constitutive model. Subsequently, numerical approaches and ABAQUS user subroutines were implemented. Furthermore, coefficient determination methods for the constitutive models were established via comparative accuracy assessments. A validated vehicle–track coupling model incorporating FACWL was developed using organized subroutines, facilitating a detailed examination of adverse load positions and influencing factors. Finally, FACWL was compared to conventional ACWL. The principal findings and conclusions are as follows:

(1) The fractional-order model outperformed the generalized Maxwell and 2S2P1D models by fitting experimental data more accurately with fewer parameters, accurately predicting viscoelastic behavior trends beyond the test frequencies, and capturing full-spectrum characteristics. Consequently, the model more effectively characterizes the temperature-dependent viscoelasticity of asphalt concrete.

(2) The structural joints of the subgrade slab represented the most critical loading points in the longitudinal direction for the dynamic response of basaltic FACWL, making them prone to stress concentration. The dynamic response of the bed FACWL extended approximately 3.1 m transversely (BS width) and 10 m longitudinally.

(3) The influence of train axle weight on the dynamic response of the roadbed surface layer was more significant and exhibited an approximately linear relationship; however, it did not influence the dynamic stress attenuation pattern within the roadbed. Additionally, temperature exerted a substantial impact on the dynamic response of the roadbed surface layer, with the relationship resembling the S-shaped main curve of the dynamic modulus.

(4) The longitudinal strain spectrum of the FACWL revealed four distinct peaks, whose frequencies primarily determined the longitudinal strain response. The dynamic modulus at these peak frequencies served as the equivalent modulus of FACWL, enabling approximate calculations of the elasticity model.

(5) Increasing the thickness of the asphalt concrete layer contributes to a reduction in the dynamic response of the subgrade bed surface layer. Taking into account dynamic performance criteria and construction costs, the recommended thickness of the asphalt concrete layer is 5–10 cm, while that of the graded crushed stone layer should be 15–30 cm.

Based on the established vehicle-track-subgrade coupled finite element model, the loading pattern of a multiple-unit train formation can be incorporated. A more accurate constitutive model may also be adopted to better characterize the stress–strain behavior between graded crushed stone and soil. This approach will enable further investigation into the influence of the asphalt concrete layer on the performance of the subgrade structure.

CRediT authorship contribution statement

Gang Xu: Writing – original draft, Data curation, Conceptualization. **You Wu:** Writing – review & editing, Writing – original draft, Visualization, Methodology, Data curation. **Wei Huang:** Writing – review & editing, Supervision, Funding acquisition, Conceptualization. **Yuefeng Shi:** Writing – review & editing. **Tianling Wang:** Writing – review & editing. **Degou Cai:** Writing – review & editing, Data curation. **Jinghong Tan:** Writing – review & editing, Writing – original draft, Investigation, Data curation. **Xianhua Chen:** Writing – review & editing, Validation, Project administration, Conceptualization.

Declaration of competing interest

The authors declare that they have no known competing financial interests or personal relationships that could have appeared to influence the work reported in this paper.

Acknowledgment

This research was Supported by the Major Science and Technology Project of Nanjing (202209012), the National Key Research and development (S&D) Program of China (2022YFB2602600), the Young Scientists Project of National Natural Science Foundation of China (52508489), the China Postdoctoral Science Foundation (2025M771642), the China Postdoctoral Science Foundation Postdoctoral Fellowship Program (GZC20240256), and the Jiangsu Funding Program for Excellent Postdoctoral Talent (2024ZB679).

Appendix A. Supplementary data

Supplementary data to this article can be found online at https://doi.org/10.1016/j.eng.2025.10.001.

References

[1] Chen X, Zhu Y, Cai D, Xu G, Dong T. Investigation on interface damage between cement concrete base plate and asphalt concrete waterproofing layer under temperature load in ballastless track. Appl Sci 2020;10(8):2654.
[2] Guimarães ACR, Filho JCS, Castro CD. Contribution to the use of alternative material in heavy haul railway sub-ballast layer. Transp Geotech 2021;30:100524.
[3] Kucera P, Lidmila M, Jasansky P, Pycha M, Burrow MPN, Ghataora GS. The feasibility of using asphalt concrete with a high percentage of recycled asphalt material in a railway trackbed layer. Transp Geotech 2021;26:100429.
[4] Fang M, Hu T, Rose JG. Geometric composition, structural behavior and material design for asphalt trackbed: a review. Constr Build Mater 2020;262:120755.
[5] Li J, Xiao X, Cai D, Lou L, Shi Y, Xiao F. Performance evaluation of composite polymerized asphalt materials for waterproofing layer in high-speed railway system. Transp Geotech 2022;37:100850.
[6] Xiao X, Cai D, Lou L, Shi Y, Xiao F. Application of asphalt based materials in railway systems: a review. Constr Build Mater 2021;304:124630.
[7] Xiao X, Li J, Cai D, Lou L, Shi Y, Xiao F. Evolution evaluation of high-speed railway asphalt concrete waterproofing layer during laboratory freeze–thaw cycles. Constr Build Mater 2022;324:126258.
[8] Liu S, Yang J, Chen X, Yang G, Cai D. Application of mastic asphalt waterproofing layer in high-speed railway track in cold regions. Appl Sci 2018;8(5):667.
[9] Yang E, Wang KCP, Luo Q, Qiu Y. Asphalt concrete layer to support track slab of high-speed railway, transportation research record. Transp Res Rec 2019;2505(1):6–14.
[10] Rose JG, Lees HM. Long-term assessment of asphalt trackbed component materials' properties and performance. In: Proceedings of the 2008 AREA Annual Conference; 2008 Sep 21–24; Salt Lake City, UT, USA. Lanham: American Railway Engineering Association (AREA); 2008.
[11] Momoya Y, Sekine E, Tatsuoka F. Deformation characteristics of railway roadbed and subgrade under moving-wheel load. Soil Found 2005;45(4):99–118.
[12] Momoya Y, Horiike T, Ando K. Development of solid bed track on asphalt pavement. Q Rep RTRI 2002;43(3):113–8.
[13] Yang E, Wang KCP, Qiu Y, Luo Q. Asphalt concrete for high-speed railway infrastructure and performance comparisons. J Mater Civ Eng 2016;28(5):0001495.
[14] Wu Y, Shi C, Yu Y, Chen H, Fan Y, Wang H, et al. Dynamic behavior of precast epoxy asphalt track bed for transition zone in high-speed railway: a numerical approach. Transp Geotech 2023;40:100960.
[15] Shi C, Sun X, Wang T, Wu Y, Liu S, Wang H, et al. Numerical analysis of dynamic behavior of bi-block precast asphalt trackbed for high-speed railway. Constr Build Mater 2022;342:128088.
[16] Shi C, Zhang H, Wang T, Zhou Y, Liu S, Wang H, et al. Design and performance evaluation of bi-block precast rubberized epoxy asphalt trackbed for railway. Constr Build Mater 2021;313:125347.
[17] Xu L, Zhai W, Zhu S, Liu W. An efficient method for train–track–substructure dynamic interaction analysis by implicit–explicit integration and multi-time-step solution. Railway Eng Sci 2022;31(1):20–36.
[18] Yang X, Yu L, Wang X, Xu Z, Deng Y, Li H. Analysis of mesoscopic mechanical dynamic characteristics of ballast bed with under sleeper pads. Railway Eng Sci 2023;32(1):107–23.
[19] Lee SH, Park DW, Vo HV, Fang M. Analysis of asphalt concrete track based on service line test results. Constr Build Mater 2019;203:558–66.
[20] Chupin O, Martin A, Piau JM, Hicher PY. Calculation of the dynamic response of a viscoelastic railway structure based on a quasi-stationary approach. Int J Solids Struct 2014;51(13):2297–307.
[21] Wu Y, Xue J, Yu Y, Shi C, Fan Y, Wang H, et al. Research of reflective crack in asphalt pavement using SCB specimen and XFEM: from laboratory test to numerical simulation. Constr Build Mater 2023;406:133419.
[22] Wang Y, Yan J, Huang W, Rutkowski L, Cao J. Variable-order fractional derivative rutting depth prediction of asphalt pavement based on the RIOHTrack full-scale track. Sci China Inf Sci 2023;66(5):152205.
[23] Zhang Q, Gu X, Dong Q, Liang J. Modified fractional-Zener model—numerical application in modeling the behavior of asphalt mixtures. Constr Build Mater 2023;388:131690.
[24] Li X, Sha A, Jiao W, Song R, Cao Y, Li C, et al. Fractional derivative Burgers models describing dynamic viscoelastic properties of asphalt binders. Constr Build Mater 2023;408:133552.
[25] Barraj F, Hatoum A, Khatib J, Assaad J, Castro A, Elkordi A. Uncertainty analysis for the dynamic modulus of recycled asphalt mixtures using unclassified fractionated RAP materials. Constr Build Mater 2024;421:135721.
[26] Padovan J. Computational algorithms for FE formulations involving fractional operators. Comput Mech 1987;2(4):271–87.
[27] Alotta G, Barrera O, Cocks A, Di Paola M. The finite element implementation of 3D fractional viscoelastic constitutive models. Finite Elem Anal Des 2018;146:28–41.
[28] Lv H, Liu H, Tan Y, Meng A, Assogba OC, Xiao S. An extended search method for identifying optimal parameters of the generalized Maxwell model. Constr Build Mater 2021;266:120796.
[29] Zhang Y, Birgisson B, Lytton RL. Weak form equation-based finite-element modeling of viscoelastic asphalt mixtures. J Mater Civ Eng 2016;28(2):0001395.
[30] Barrientos E, Pelayo F, Noriega Á, Lamela MJ, Fernández-Canteli A, Tanaka E. Optimal discrete-time Prony series fitting method for viscoelastic materials. Mech Time-Depend Maters 2019;23(2):193–206.
[31] Wang H, Markine V. Dynamic behaviour of the track in transitions zones considering the differential settlement. J Sound Vibr 2019;459:114863.
[32] Shen C, Zhang P, Dollevoet R, Zoeteman A, Li Z. Evaluating railway track stiffness using axle box accelerations: a digital twin approach. Mech Syst Signal Proc 2023;204:110730.
[33] Cai X, Zhang Q, Wang Q, Cui X, Dong B. Effects of the subgrade differential arch on damage characteristics of CRTS III slab track and vehicle dynamic response. Constr Build Mater 2022;327:126982.
[34] Humar JL. Dynamics of structures. 3rd ed. Raton: CRC Press; 2012.
[35] Feng SJ, Zhang XL, Wang L, Zheng QT, Du FL, Wang ZL. In situ experimental study on high speed train induced ground vibrations with the ballast-less track. Soil Dyn Earthq Eng 2017;102:195–214.
[36] Xu L, Zhai W. Train–track coupled dynamics analysis: system spatial variation on geometry, physics and mechanics. Railway Eng Sci 2020;28(1):36–53.
[37] Wang H, Markine VL. Methodology for the comprehensive analysis of railway transition zones. Comput Geotech 2018;99:64–79.
[38] Shih JY, Thompson D, Zervos A. The effect of boundary conditions, model size and damping models in the finite element modelling of a moving load on a track/ground system. Soil Dyn Earthq Eng 2016;89:12–27.
[39] Chen J, Zhou Y. Dynamic vertical displacement for ballastless track-subgrade system under high-speed train moving loads. Soil Dyn Earthq Eng 2020;129:105911.
[40] Bodin D, Chupin O, Denneman E. Viscoelastic asphalt pavement simulations and simplified elastic pavement models based on an "equivalent asphalt modulus" concept. J Test Eval 2017;45(6):1887–95.